UvA-DARE (Digital Academic Repository)

Crossing muscle fibers of the human tongue resolved in vivo using constrained spherical deconvolution

Voskuilen, L.; Mazzoli, V.; Oudeman, J.; Balm, A.J.M.; van der Heijden, F.; Froeling, M.; de Win, M.M.L.; Strijkers, G.J.; Smeele, L.E.; Nederveen, A.J.

Crossing Muscle Fibers of the Human Tongue Resolved In Vivo Using Constrained Spherical Deconvolution

Luuk Voskuilen, MSc,[1,2,3]* Valentina Mazzoli, PhD,[4] Jos Oudeman, MD, PhD,[2]

Alfons J.M. Balm, MD, PhD,[1,5,6] Ferdinand van der Heijden, PhD,[1,6]

Martijn Froeling, PhD,[7] Maartje M.L. de Win, MD, PhD,[2] Gustav J. Strijkers, PhD,[8]

Ludi E. Smeele, MD, PhD,[1,5] and Aart J. Nederveen, PhD[2]

Background: Surgical resection of tongue cancer may impair swallowing and speech. Knowledge of tongue muscle architecture affected by the resection could aid in patient counseling. Diffusion tensor imaging (DTI) enables reconstructions of muscle architecture in vivo. Reconstructing crossing fibers in the tongue requires a higher-order diffusion model.
Purpose: To develop a clinically feasible diffusion imaging protocol, which facilitates both DTI and constrained spherical deconvolution (CSD) reconstructions of tongue muscle architecture in vivo.
Study Type: Cross-sectional study.
Subjects/Specimen: One ex vivo bovine tongue resected en bloc from mandible to hyoid bone. Ten healthy volunteers (mean age 25.5 years; range 21–34 years; four female).
Field Strength/Sequence: Diffusion-weighted echo planar imaging at 3 T using a high-angular resolution diffusion imaging scheme acquired twice with opposing phase-encoding for B_0-field inhomogeneity correction. The scan of the healthy volunteers was divided into four parts, in between which the volunteers were allowed to swallow, resulting in a total acquisition time of 10 minutes.
Assessment: The ability of resolving crossing muscle fibers using CSD was determined on the bovine tongue specimen. A reproducible response function was estimated and the optimal peak threshold was determined for the in vivo tongue. The quality of tractography of the in vivo tongue was graded by three experts.
Statistical Tests: The within-subject coefficient of variance was calculated for the response function. The qualitative results of the grading of DTI and CSD tractography were analyzed using a multilevel proportional odds model.
Results: Fiber orientation distributions in the bovine tongue specimen showed that CSD was able to resolve crossing muscle fibers. The response function could be determined reproducibly in vivo. CSD tractography displayed significantly improved tractography compared with DTI tractography ($P = 0.015$).
Data Conclusion: The 10-minute diffusion imaging protocol facilitates CSD fiber tracking with improved reconstructions of crossing tongue muscle fibers compared with DTI.
Level of Evidence: 2
Technical Efficacy: Stage 1

*Address reprint requests to: L.V., Department of Head and Neck Oncology and Surgery, Netherlands Cancer Institute, Antoni van Leeuwenhoek Hospital, Plesmanlaan 121, 1066CX Amsterdam, The Netherlands. E-mail: l.voskuilen@nki.nl

From the [1]Department of Head and Neck Oncology and Surgery, Netherlands Cancer Institute, Antoni van Leeuwenhoek Hospital, Amsterdam, Netherlands; [2]Department of Radiology and Nuclear Medicine, Amsterdam UMC, University of Amsterdam, Amsterdam, Netherlands; [3]Department of Oral and Maxillofacial Surgery, Academic Centre for Dentistry Amsterdam and Amsterdam UMC, University of Amsterdam and VU University Amsterdam, Amsterdam, Netherlands; [4]Department of Radiology, Stanford University, Stanford, CA, USA; [5]Department of Oral and Maxillofacial Surgery, Amsterdam UMC, University of Amsterdam, Amsterdam, Netherlands; [6]Department of Robotics and Mechatronics, MIRA Institute, University of Twente, Enschede, Netherlands; [7]Department of Radiology, University Medical Center Utrecht, Utrecht, Netherlands; and [8]Department of Biomedical Engineering and Physics, Amsterdam UMC, University of Amsterdam, Amsterdam, Netherlands

CARCINOMAS INVOLVING THE TONGUE are preferably removed surgically.[1] The amount of resected tissue, which can be substantial, is associated with loss in tongue functionality affecting speech,[2] mastication, and swallowing.[3] The location and type of resection play a prominent role in the expected extent of loss of functionality.[4] Detailed insights into how individual tongue muscles are involved in complex tongue functionality such as speech and swallowing, however, are lacking, especially in the presence of a tumor. Therefore, some might want to study the complex tongue muscle anatomy in vivo.

This complex tongue muscle anatomy is comprised of intrinsic and extrinsic muscle groups. The intrinsic musculature of the tongue belongs to the category of muscular hydrostats,[5] consisting of transverse (TRA) and vertical (VER) muscles, surrounded by longitudinally oriented fibers (superior longitudinal [SL] and inferior longitudinal [IL] muscles).[5,6] Furthermore, the tongue contains four extrinsic muscles (genioglossus [GG], hyoglossus [HG], styloglossus [SG], and palatoglossus [PG] muscles), which originate from the mandible, hyoid bone, styloid process of the skull, and the palate, respectively.[7] To predict the functional outcome after surgical resection in such complex musculature, one cannot simply rely on experience or common imaging modalities.[8] To better model and understand residual functionality after surgery, it is essential to obtain the muscular architecture on an individual patient basis, especially the musculature that is to be resected.

Diffusion weighted imaging (DWI) has been used as a non-invasive method to image tongue muscular architecture in vivo.[9] DWI is capable of quantifying the self-diffusion of water in biological tissues by measuring the attenuation of the magnetic resonance imaging (MRI) signal in the presence of diffusion-encoding gradients. Diffusion of water in skeletal muscle is anisotropic[10]: Perpendicular to muscle fibers, water diffusion is restricted by cell membranes as well as by structured intracellular and extracellular proteins, whereas along the muscle fibers water molecules diffuse more freely.

In diffusion-tensor imaging (DTI), this orientation dependence of diffusion is geometrically described by a rank-2 semi-definite positive tensor. The first eigenvector of the diffusion tensor, which corresponds to the largest eigenvalue, has been shown to align with the local muscle fiber direction in skeletal muscle.[11] In a technique called tractography, the principal diffusion vectors of individual voxels are connected via streamlines, which results in 3D reconstructions of the underlying muscle architecture.[12]

A drawback of DTI is that the diffusion tensor can only describe a single fiber orientation per voxel. However, due to the relatively large voxel size in DWI compared with the diameter of the myocytes, multiple muscle fiber population appear to cross or merge within a voxel. This is particularly relevant for the tongue, due to its complex structure with many crossing muscle fibers. DTI is therefore generally not capable of resolving the true tongue muscle architecture.

Crossing fibers can be resolved, though, by higher-order diffusion models, such as by constrained spherical deconvolution (CSD).[13] CSD is based on the assumption that a fiber orientation distribution (FOD) can be calculated by deconvolution of the measured DWI signal and a response function (RF), which corresponds to the DWI signal of a single fiber population.[14] The FOD, DWI signal, and RF are described using spherical harmonics. Therefore, a maximum harmonic order (l_{max}) has to be defined, where a higher l_{max} allows a higher maximal angular resolution to be obtained. Additionally, a peak threshold is chosen to remove small spurious peaks in the calculated FOD.

While for DTI the measurement of six noncollinear diffusion directions is theoretically sufficient, CSD requires sampling of the diffusion along many more directions. The minimal number of gradient directions required is defined by $n_{\min} = \frac{1}{2}(l_{\max} + 1)(l_{\max} + 2)$; thus, for l_{max} = 8 at least 45 unique gradient directions are necessary. Therefore, the diffusion sampling strategy required for CSD is referred to as high-angular resolution diffusion imaging (HARDI).[15] Application of this approach to the human tongue is not straightforward, since measurements of many diffusion directions necessitates a long scan time. Such a long scan time for tongue imaging is undesirable, due to signal dropouts from motions such as involuntary swallowing. In DWI, the scan time is commonly reduced by using an echo-planar imaging (EPI) readout, and because other acceleration techniques such as multishot imaging introduce motion-related phase errors.

A major disadvantage of spin-echo (SE)-EPI is the small bandwidth per voxel in the phase-encoding direction, which increases the susceptibility to B_0-inhomogeneity artifacts. Therefore, air–tissue interfaces and metal-based dental prostheses, which distort the B_0-field, will result in deformations in the phase-encoding direction. These distortions can be corrected for by using an algorithm from the FSL library, Topup.[16] Topup estimates the inhomogeneity field by estimating the distortions, which are equal in magnitude but opposite in direction, between two DWI datasets acquired with opposite phase-encoding directions. Subsequently, the two images are combined, partially restoring spatial encoding information lost in the distorted images due to signal pile-up, using information from the opposite image, where the signal is dispersed.[16]

The aim of this study was to develop a clinically feasible scan protocol and postprocessing pipeline for reconstructing the complex muscular architecture of the human tongue in vivo allowing both DTI and CSD fiber tractography.

Materials and Methods

Bovine Tongue Specimen

One ex vivo bovine tongue was acquired from a local slaughterhouse. The specimen was resected en bloc from mandible and hyoid bone.

The imaging of the tongue was performed within 24 hours after harvest. The bovine tongue (~45 cm in length) was cast into alginate polymer before scanning. The alginate cast reduced B_0-inhomogeneity, and provided support for the tongue to minimize deformation due to the weight of the coil.

Imaging of Bovine Tongue

Standard torso (16 channels) and posterior coils (12 channels) were used for acquisition on a 3 T Ingenia scanner (Philips Medical Systems, Best, The Netherlands). Diffusion-weighted images were acquired using a HARDI[15] gradient scheme, in which 64 diffusion directions were evenly spaced over a sphere, optimized for gradient load.[17] Although 45 gradient directions are theoretically sufficient for $l_{max} = 8$, we acquired more diffusion directions to reduce the susceptibility of the calculated FODs to noise. A b-value of 1000 s/mm^2 was used, which is higher than the b-value for the in vivo acquisitions to compensate for the loss of diffusivity postmortem. After every eight diffusion-weighted images one b0-image was acquired. All images were acquired with two opposing phase-encoding directions, RL and LR. Other imaging parameters were: SE-EPI; echo train length (ETL): 31; field of view (FOV): 192 (AP) × 154 (RL) × 420 (FH) mm^3; voxel size: 2.4 × 2.4 × 2.4 mm^3; matrix size: 80 × 62; echo time (TE): 68 msec; repetition time (TR) = 40.5 sec; SENSE: 2; no partial Fourier; bandwidth per pixel in the phase-encoding direction: 46.4 Hz; number of signal acquired (NSA): 1; SPIR and SSGR fat suppression; scan time: 2 hours.

Volunteers

Ten healthy volunteers (mean age 25.5 years; range 21–34 years; 4 female) were scanned. All volunteers provided written informed consent. Volunteers were excluded if a contraindication for MRI or orthodontic braces was present. This study was approved by the institutional Ethics Committee Review Board.

In Vivo Imaging

Two flexible surface coils, 20 cm in diameter, were gently strapped to the cheeks of the volunteers for acquisition on a 3 T Ingenia scanner (Philips Medical Systems). The scan protocol was repeated with an interval of no more than 10 minutes between scans to assess reproducibility. In between the two scans, the volunteer left the table and was repositioned. During scanning, volunteers were instructed to let their tongue rest against their palate, stabilizing the tongue and removing as much excessive air from the oral cavity as possible.

The same diffusion gradient scheme as for the ex vivo experiment with 64 diffusion-encoding directions was divided into two sets of 32 directions in order to maintain an equally spaced distribution. Other imaging parameters were: SE-EPI; ETL: 25; FOV: 192 (AP) × 156 (RL) × 84 (FH) mm^3; voxel size: 3 × 3 × 3 mm; matrix size: 64 × 49; TE: 60 msec; TR: 3.4 sec; SENSE: 2; no partial Fourier; bandwidth per pixel in the phase-encoding direction: 56.4 Hz; NSA: 1; SPIR and SSGR fat suppression; b-value: 700 s/mm^2; scan time: 10:03 minutes. The total scan protocol consisted of four parts (phase-encoding: RL&LR and 2 × 32 gradient directions) of 2:30 minutes each. In between these parts, we allowed the volunteer to swallow. This approach minimized tongue motion due to the swallowing reflex initiated by the build-up of saliva in the oral cavity.

Data Processing

Diffusion-weighted images were smoothed with a Rician noise filter in DTITools for Mathematica.[12] The B_0-inhomogeneity field was estimated using the previously described Topup. Subsequently, the DWIs were corrected for inhomogeneity, rigid motion, and eddy currents using FSL.[18] A mask of the whole ex vivo tongue was created by applying a threshold including the top 95% voxels regarding intensity of the corrected b0-image. Masks of the in vivo tongues were defined by manually delineation in ITK-Snap[19] on the corrected b0-images. These masks reduced computation time and served as an outer boundary for tractography.

For both ex vivo and in vivo data, diffusion tensors were fitted using RESTORE,[20] and fractional anisotropy (FA) and mean diffusivity (MD) were calculated in ExploreDTI.[21] The average FA and MD were calculated for a manually delineated region of interest (ROI) in the GG muscle in a known noncrossing area. The diffusion signal in spherical harmonic representation of voxels exceeding these average FA and MD values were averaged to obtain the CSD response function (RF). FODs were subsequently calculated in the entire tongue using $l_{max} = 8$, which was chosen to obtain the largest angular resolution in the FODs possible.

For the in vivo data, whole tongue deterministic DTI tractography was performed using the following parameters chosen empirically: FA range: 0.1–0.6; seed point resolution: 3 mm; step size: 1 mm; angular threshold: 15°; tract length: 10–100 mm.

We performed a Bland–Altman analysis on the two repeated measurements of the FA and MD that are used to define the RF. Additionally, the interscan variability was determined by calculating the within-subject coefficient of variation (wsCV) by dividing the standard deviation of the paired difference by the mean of the paired average.

In muscular tissues, the diffusion anisotropy is generally much lower than in brain tissue.[22] Therefore, the RF in muscles is more spherical, increasing the susceptibility to overfitting and thus spurious peaks in FODs. In order to minimize the effects on in vivo tractography of these spurious peaks, which are generally smaller than true peaks, an FOD peak threshold is employed. This peak threshold removes peaks shorter than the peak threshold times the length of the largest peak. We determine the optimal FOD peak threshold[23] by calculating the number of peaks per voxel for 10 different peak thresholds ranging from 0.05–0.50. The number of voxels containing three peaks, which may be considered spurious, false-positive peaks, has to be minimized. However, a peak threshold that is too high results in an increasing number of false-negative peaks, mainly in voxels with crossing fibers that should contain two peaks. A tradeoff has to be made between false-positive and false-negative peaks.

Finally, whole tongue deterministic CSD tractography was performed in ExploreDTI with an FOD peak threshold of 0.10. The other tracking parameters were the same as for deterministic DTI tractography, however, without the FA constraint. Representative images of DTI and CSD tractography for both repetitions and all 10 subjects were graded by three reviewers on a three-point ordinal scale, where three is the best and one the worst grade. Tractography of the tongue is rare and therefore the reviewers had limited experience with these images. Therefore, two reviewers were chosen with extensive knowledge of tongue muscular anatomy (head and neck surgeons) and one reviewer experienced in brain DTI
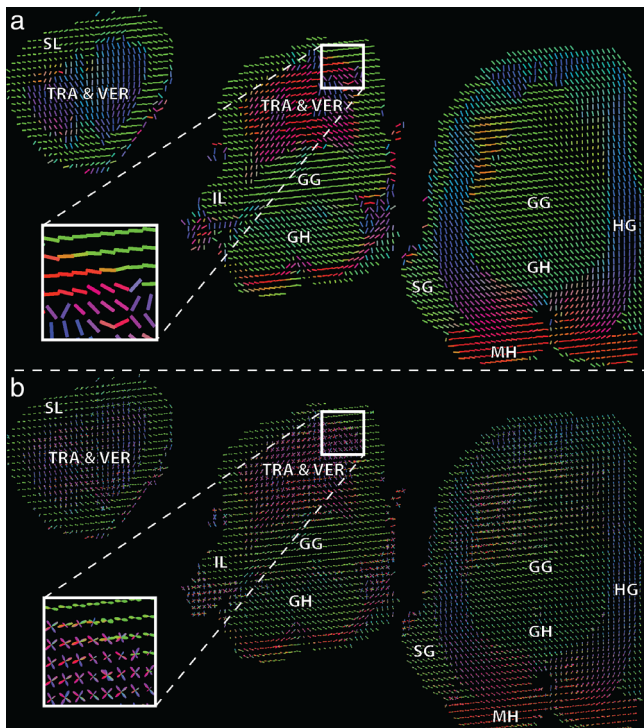
FIGURE 1: Fiber directionality of the bovine tongue determined by the primary eigenvector of DTI (a) and the fiber orientation distribution of CSD (b), color-coded similarly to the human tongue (red: right-left, green: cranio-caudal, blue: anterior-posterior). The following muscles are annotated in the slices: superior longitudinal (SL); transverse (TRA); vertical (VER); genioglossus (GG); inferior longitudinal (IL); geniohyoid (GH); hyoglossus (HG); styloglossus (SG); mylohyoid (MH). The white boxes indicate the location of the inlays, which highlight to ability of CSD to resolve crossing fibers of TRA and VER, while maintaining the correct reconstruction of single fibers of the SL.

(radiologist). Five questions were asked: "Can you grade the overall quality of the data", "How well can you distinguish the transverse & vertical muscles?", "How well can you distinguish the hyoglossus and styloglossus?", "How well can you appreciate the superior longitudinal muscle?", "How would you grade the influence of gaps in tractography on the image quality?"

The grades provided by the expert reviewers were modeled using a multilevel proportional odds model in R using the ordinal package.[24] We modeled the grades given by the expert reviewers using the method (DTI or CSD) and repetition as fixed effects, and subjects, expert reviewers, and the five asked questions as random effects with random intercepts. Random slopes were used for

variables reviewers and questions regarding the method (DTI or CSD). *P*-values of the effect of using DTI or CSD and the effect of repetition were calculated by likelihood ratio tests of the full model compared with models without either the method or repetition as fixed effects.

Results

In the bovine tongue specimen (Fig. 1), DTI primary eigenvectors and FOD display similar fiber directionality in noncrossing muscles such as the HG, SG, and GH muscles. However, the enlarged sections of the intrinsic tongue musculature show that DTI (Fig. 1a) is unable to distinguish between TRA and VER muscles. The CSD FODs (Fig. 1b) show two peaks, which indicates that CSD appears to be able to distinguish the TRA and VER muscles. On the interface between the TRA, VER, and SL, where a partial volume effect is present in three muscle directions, three peaks corresponding to these three muscles can be appreciated.

In all 10 volunteers, both repetitions of the DWI acquisition were acquired successfully without any subject dropouts due to, for example, tongue motion. Figure 2 shows the effect of inhomogeneity correction using Topup on transverse diffusion-weighted images of a single in vivo tongue, where inhomogeneity artifacts are clearly present. Distinct but opposite distortions of b0-images are present along the phase-encoding direction (RL & LR, Fig. 2a,b). The estimated B_0-inhomogeneity map (Fig. 2c) displays field inhomogeneity at expected locations due to differences in magnetic field permeability, ie, at tissue–tooth interfaces, laterally to the tongue, and at air–tissue interfaces, near the oropharynx and skin. The inhomogeneity map was used to combine and correct the images with opposite phase-encoding, resulting in the corrected images (Fig. 2d), which correspond better to the actual morphology of the tongue (Fig. 2e).

The Bland–Altman analysis of two repeated measurements of the FA and MD used for RF estimation is displayed in Fig. 3. For the two DTI metrics defining the RF, the bias is close to zero, suggesting that the systematic error in determining the RF is low. The wsCV was 7.3% for FA and 3.3% for MD.

Figure 4a shows the percentage of voxels with one, two, or three peaks as a function of FOD peak threshold. The

FIGURE 2: B_0-inhomogeneity correction using Topup. a: Transverse b0-image with phase encoding along the left-right direction. b: Similar b0-image with phase encoding opposite to a. Image distortions are present along the phase-encoding direction but opposite between a and b; for example, lateral to the tongue (white arrows). c: B_0-inhomogeneity map estimated by Topup. Strong inhomogeneities are present at air–tissue interfaces and near teeth lateral to the tongue (white arrow). d: Resulting combined b0-image with corrected for B_0-inhomogeneity. e: T_2-weighted Dixon image serving as a high-resolution undistorted gold standard for the distortion correction.
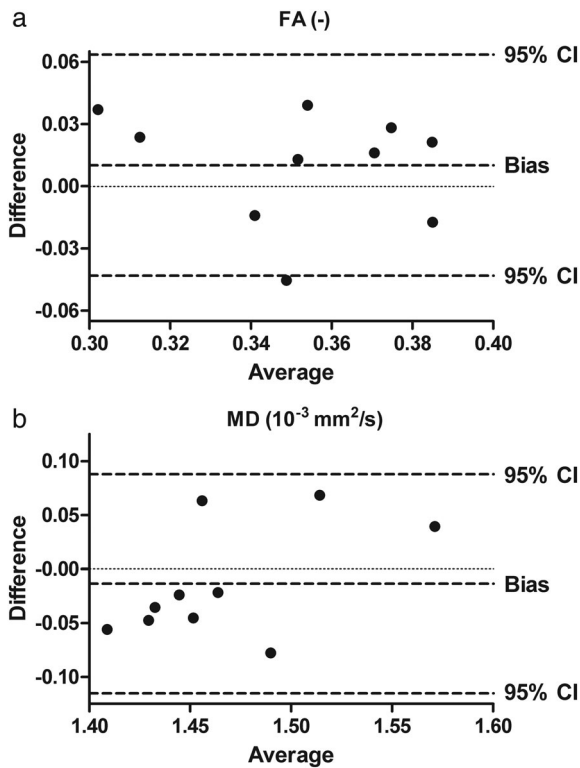
FIGURE 3: Bland–Altman plots of FA and MD used to estimate the CSD response function (RF) using two repeated measurements for 10 healthy volunteers. The RF was determined by drawing an ROI in the GG muscle, where only one fiber direction is present. The two metrics, FA (a) and MD (b) that define the RF were calculated by fitting a diffusion tensor.

removed to improve visibility of the crossing fibers of the tongue core.

DTI and CSD tractography of two typical volunteers is compared with textbook anatomy[25] in Fig. 6. The TRA muscle fibers and fibers in the tip of the tongue are missing in DTI tractography. Additionally, the extrinsic muscles SG and HG appear to have merged in the DTI tractography, while these muscles cross in CSD tractography, the latter of which is in accordance with textbook anatomy. Finally, CSD tractography displays spurious tracts, which are not visible in DTI tractography.

The proportion of the grades given by the expert reviewers for both DTI and CSD are summarized in Fig. 7. Images of
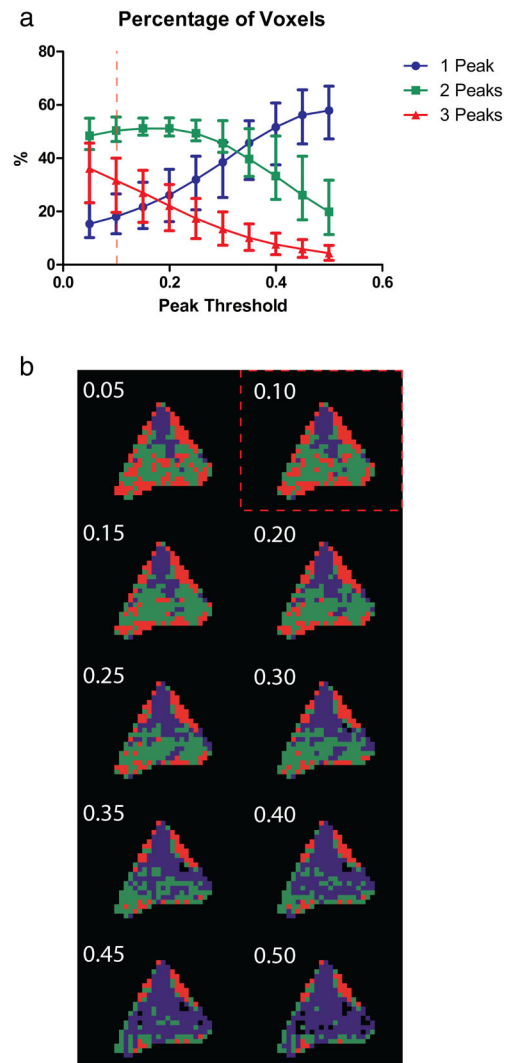
FIGURE 4: The effect of changing the peak threshold on the percentage of voxels with one, two, or three peaks on all volunteers (a); brackets represent the range of percentages. The spatial distribution of the number of peaks per voxel in a single volunteer (b) colored similarly to a. Note that increasing the peak threshold decreases the number of 3-peak-voxels, which generally contain spurious peaks. However, increasing the peak threshold also decreases the number of two-peak-voxels in the center of the tongue, therefore reducing the ability of resolving crossing muscle fibers.
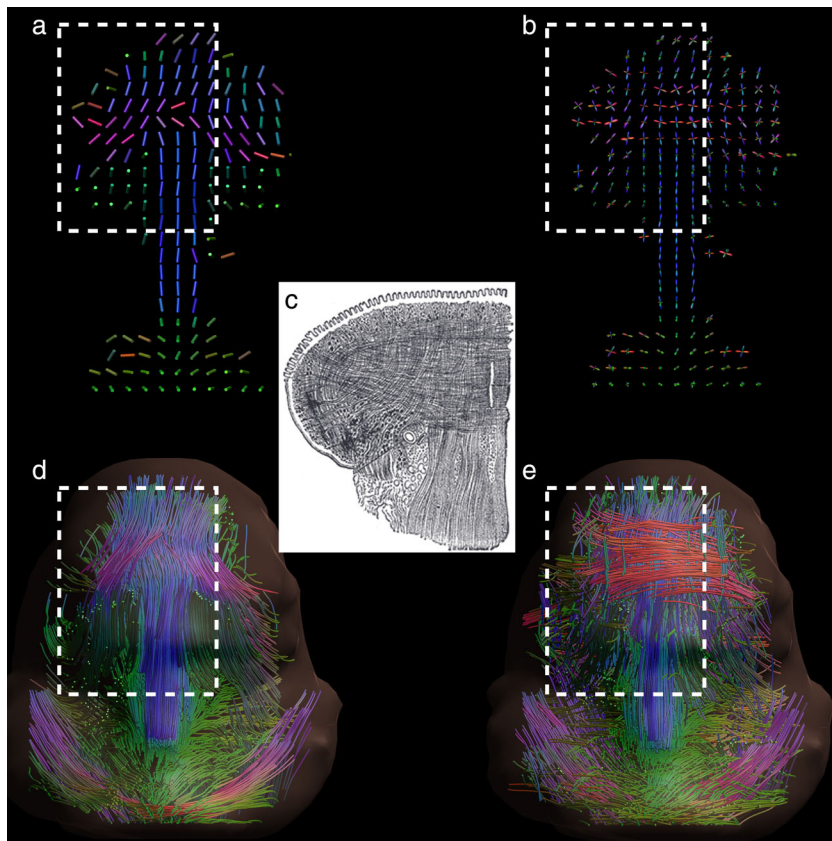
percentage of voxels with two peaks reaches a maximum around 0.15, suggesting that a peak threshold of 0.15 is ideal for resolving two crossing muscle fibers, which most commonly occurs in the tongue. An example of the spatial distribution of the number of peaks per voxel in a single transverse slice is displayed in Fig. 4b. The three-peak-voxels, which may be considered to contain spurious, false-positive peaks, are mainly located in the periphery and are therefore of little influence on tractography. However, a peak threshold of 0.15 or higher results in an increasing number false-negative peaks, namely, the number of voxels in the posterior part of the tongue containing only one peak. The latter does impact tractography; thus, a peak threshold of 0.10 was chosen as a reasonable compromise between false-positive and false-negative peaks.

The coronal view of one in vivo human tongue (Fig. 5) illustrates the ability of CSD to resolve crossing fibers in the tongue core in vivo contrary to DTI. The images of FODs and CSD tractography both more closely resemble the anatomical atlas compared with their DTI counterparts. The DTI principal eigenvectors in the TRA & VER muscles appear to be an oblique average of the two FOD peaks. Note that fiber tracts belonging to the tip of the tongue for both DTI and CSD have been

FIGURE 5: Coronal view of in vivo DTI and CSD fiber directionality and tractography in a healthy volunteer compared with textbook anatomy.[25] Images are conventionally color-coded (red: right–left, green: anterior–posterior, blue: inferior–superior). a: Coronal slice of the in vivo human tongue displaying the primary eigenvector of the diffusion tensor as a color-coded cylinder. b: Coronal slice identical to (a) but displaying FODs calculated by CSD. c: Illustration (adapted from Gray's Anatomy) of a coronal slice of the human tongue displaying crossing transverse and vertical muscle fibers. d: Coronal view of DTI fiber tractography. e: Coronal view of CSD fiber tractography. The areas corresponding to the slice from the anatomical atlas have been marked. In (d,e), fibers originating from the apex of the tongue have been removed to improve the visibility of the crossing fibers in the tongue core.

CSD tractography have significantly higher odds of being graded higher than images of DTI tractography (P = 0.015). These odds were not significantly different between the two repetitions (P = 0.161). Images of CSD and DTI tractography that were graded by expert reviewers can be found in Fig. 8.

Discussion

In this study we created a scan protocol and processing pipeline for human in vivo CSD tractography within a clinically acceptable scan time of 10 minutes. CSD allow more accurate reconstructions of tongue musculature in regions containing crossing fibers compared with DTI tractography in vivo and ex vivo. However, CSD tractography is more susceptible to erroneous fibers due to the presence of spurious peaks.

The ex vivo mammalian tongue has been a frequently used model to test higher-order diffusion models in the past,[26–28] arguably due to the better conservation of crossing fibers postmortem compared with brain tissue. Diffusion spectrum imaging (DSI) has been successfully used to resolve the crossing fibers of the transverse and vertical muscles, and the surrounding sheet of longitudinal muscles in the bovine[26] and murine[27] ex vivo

tongue. In the latter example, Gaige et al were also able to relate DSI tractography and microscopy.[27] We were able to reconstruct a similar muscular architecture (containing transverse, vertical, and longitudinal fibers) in the bovine tongue as these previous DSI experiments; thus, we suppose that CSD is also able to correctly capture the complex tongue architecture ex vivo.

For human measurements, we could not find such a "gold standard". Therefore, we could not validate our results, except for the comparison with textbook anatomy. Although DSI has been validated ex vivo, the relatively high number of gradient directions and high maximum b-values require a long scan time; for example, ~25 minutes for a single slice with a b-value of 8000 s/mm^2.[29] This excessively long scan time makes DSI unsuitable for a clinical setting. Another diffusion model, generalized q-space imaging (GQI), also has the ability to discern between crossing muscle fibers in the murine tongue[28] using a similar HARDI scheme and scan time as CSD. However, the typical array of transverse, vertical, and longitudinal fibers could only be detected in the murine model and not in the in vivo human case. This absence may be caused by B$_0$-inhomogeneities, which were not accounted for, or by the lower angular resolution of GQI
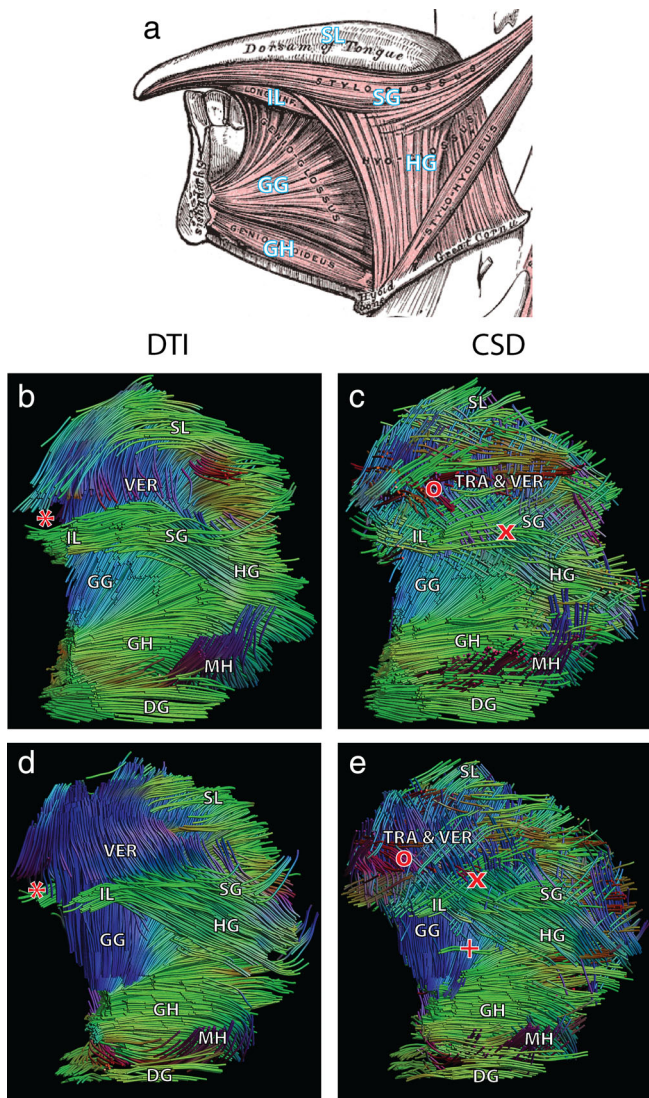
FIGURE 6: Textbook anatomy[25] (a) compared with DTI and CSD tractography of volunteers 9 (b,c) and 5 (d,e) in a frontosagittal view. The following muscles of the tongue and floor of the mouth have been annotated: superior longitudinal (SL); transverse (TRA); vertical (VER); inferior longitudinal (IL); styloglossus (SG); genioglossus (GG); hyoglossus (HG); geniohyoid (GH); mylohyoid (MH); digastric (DG). DTI tractography is unable to reconstruct the tip of the tongue in these cases (*). CSD tractography is able to resolve transverse fibers (o) in the tongue; however, DTI tractography cannot. In DTI tractography the SG and HG are merged into a single fiber bundle, while CS is able to resolve both muscles (x). An example of spurious tracts is present in CSD tractography (+).

compared with CSD, as shown in computer simulations.[30] Therefore, we deem CSD to be a reasonable compromise between accuracy in resolving crossing fibers and scan time.

Gaige et al previously used DTI to determine the human tongue muscular architecture in vivo.[9] Due to the inherent limitation of the tensor model, namely, only one fiber direction per voxel, crossing fibers from the transverse muscle fibers could not be detected. The vertical fibers appear slightly oblique, similar to our findings with in vivo DTI tractography. These similarities suggest that the acquired data are

similar to previous work, but that the diffusion tensor is an insufficient model to describe tongue muscular architecture. However, the present imaging protocol requires a substantial increase in scan time compared with an imaging protocol designed only for DTI. Future studies need to prove whether the additional information gained by CSD are worth the additional scan time required.

DTI of patients following partial glossectomy has been performed;[31,32] however, the tongue musculature superior to the IL muscle was not reported. Due to the crossing nature of the muscle fibers and the influence of B_0-inhomogeneities, we suspect that these muscles could not be reconstructed. In another case, prior information from a manually segmented high-resolution anatomical image was used to fit a multitensor model to a DTI acquisition scheme.[33] Although this method allows for the reconstruction of the crossing transverse and vertical fibers in a limited scan time, this method is highly dependent on prior knowledge. This prior is created manually and might not always be correct, for example with variations between subjects.

In the present study the RF was determined by calculating the average FA and MD in a single fiber ROI of the GG muscle. Comparing the present reproducibility to the human forearm,[34] the wsCV of the FA appears to be similar, while the wsCV of the MD appears to be better for the ROI in the GG. Although the RF is determined in a reproducible manner by manual delineation in the GG, this RF might not be the most suitable RF for other tongue muscles due to differences in muscle fiber diameter and fiber type composition. Methods of automatically determining the RF have been developed for brain CSD.[35,36] These methods are designed to circumvent the fact that in the brain few voxels contain a single fiber direction, while these voxels are more prevalent in muscle diffusion imaging. Nonetheless, we recommend adapting such an automatic method to muscle CSD, because of the less user input required and possibly increased reproducibility of RF estimation due to variation between tongue muscles.

To minimize the number of spurious peaks caused by the more spherical RF due to the low FA in muscle CSD compared with brain CSD, the FOD peak threshold has to be chosen carefully. We chose a relatively low peak threshold so the number of false-negative peaks will be low. We assume that the false-positive peaks will have a limited effect on the final tractography results, because spurious peaks tend to have a large angular difference with surrounding voxels, and therefore have a higher chance of being ignored during tractography. Nevertheless, spurious tracts do appear in the final tractography results. To further reduce the number of spurious tracts, we suggest using a higher b-value, which results in a sharper RF taking into account that sufficient signal-to-noise ratio (SNR) is maintained,[36] or improving the SNR.[35]
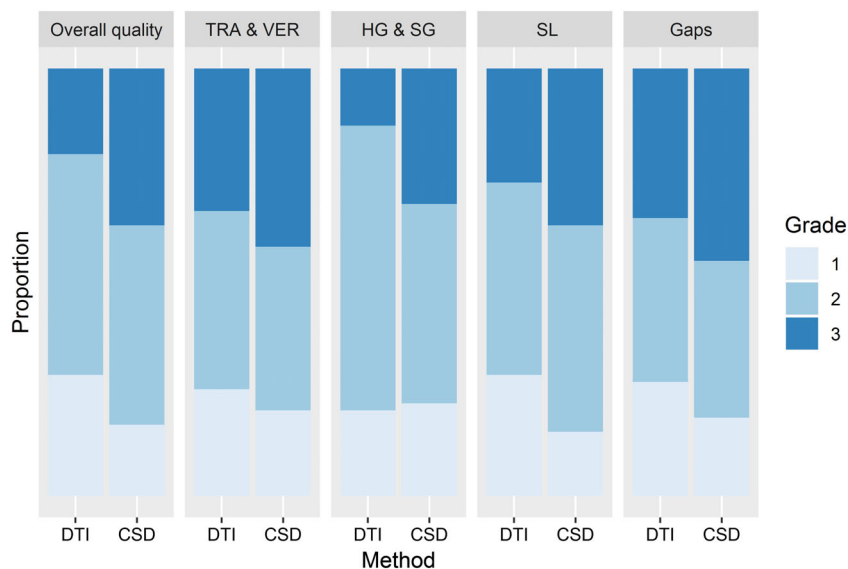
FIGURE 7: Visualization of the distribution of the selected grades for evaluating the quality of CSD and DTI, where three is the best and one the worst grade. Note that the data from all expert reviewers and both repetitions are included here. Five questions were asked focused on overall quality of the data and the visualization of crossing muscles. The odds of receiving a higher grade is significantly higher ($P = 0.015$) for CSD compared with DTI, while no such difference was detected between the two repetitions ($P = 0.161$).

The SNR may be increased by increasing the number of signal averages, which will lead to a longer scan time, and therefore a higher chance of motion artifacts. We optimized the SNR using our current hardware by using two flexible surface coils strapped to the cheeks of the volunteers instead of the standard neurovascular coil. However, custom-built receive coils have been shown to improve SNR,[37] which may reduce the number of spurious peaks, or which may increase spatial resolution to reduce the partial volume effect.

We used a high b-value of 700 s/mm^2 compared with other DTI studies of muscle, but low compared with CSD studies of the brain. Our chosen b-value is a trade-off between the high b-value necessary for a high angular resolution for CSD,[30] and a short TE to obtain sufficient SNR in muscular tissue, which has a comparatively short T_2 compared with gray and white matter. Because the diffusivity of brain[38] tissue is approximately half the magnitude of muscular tissue,[12] the b-value used in this study (700 s/mm^2) compares approximately to a b-value of 1400 s/mm^2 in the brain, which is in the range of typically used b-values.

In the present study we were able to reconstruct most tongue muscles except for the smallest extrinsic muscle: the
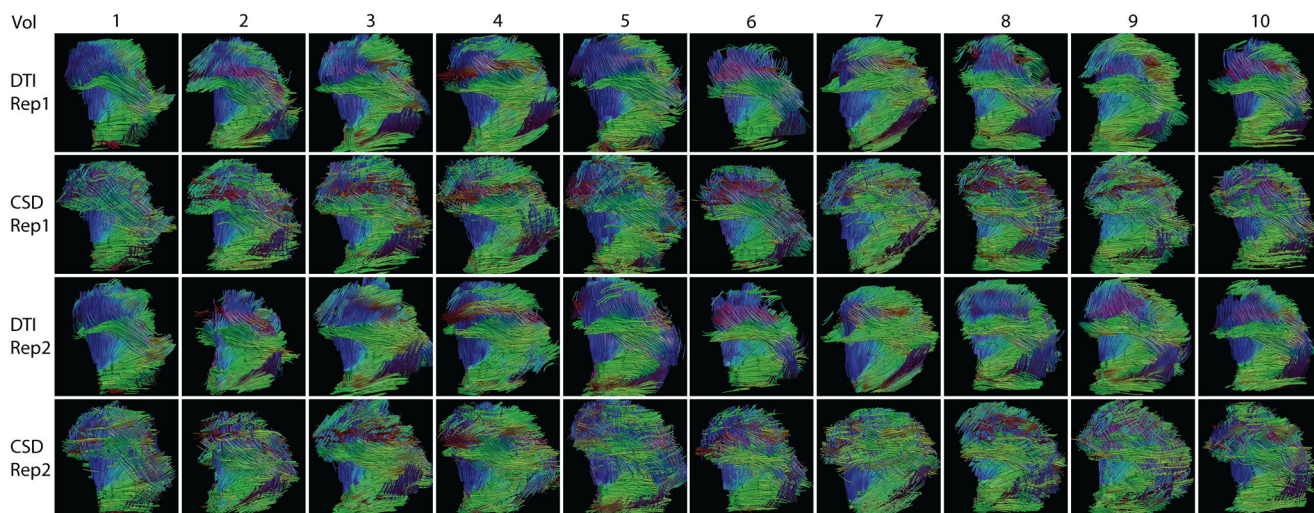
FIGURE 8: Sagittal/oblique images of DTI and CSD tractography of the 10 volunteers (Vol) for the first (Rep1) and second (Rep2) acquisitions. These images were used for the qualitative grading by three expert reviewers. Similar to Fig. 5, transverse muscle fibers are better reconstructed in CSD tractography compared with DTI tractography. The SL is also represented better in CSD tractography; however, CSD tractography is more prone to spurious tracts than DTI tractography. Note that in some cases of DTI tractography, the tip of the tongue is missing (vol0, vol5, vol6, vol7, vol9).

PG. Most probably, the PG muscle merges with the styloglossus muscle nearly immediately after insertion in the body of the tongue,[6] hindering the differentiation between each other. The PG muscle could also be missed due to the fact that tractography was constrained to the whole tongue masks. Additionally, the origins of the PG and SG muscles (the styloid process and soft palate, respectively) were not imaged to reduced scan time. As reported previously,[32] we also could not distinguish the IL from the SG muscles in vivo. Anatomical dissection has shown that the parallel fiber bundles of these two muscles are even difficult to distinguish on a microscopic level, especially near the apex of the tongue.[6,39] Finally, we had difficulties in tracking the SL. The relatively large voxel size causes a partial volume effect that may terminate SL fiber tracking prematurely. Also, normal breathing of the subjects, causing slight deviations of the base of tongue over time, which contributed to impairment of reconstruction of the SL muscle in the posterior tongue.

Three expert reviewers graded images for both DTI and CSD tractography in five categories. Additionally, a limited three-point scale was chosen, because the ability of discerning between more than three points comes with experience. Unfortunately, this limited scale also reduces the power of the statistical analyses. It was therefore not feasible to obtain meaningful qualitative results on questions individually with only 10 subjects.

During acquisition, B_0-inhomogeneity distortions were minimized by exclusion of volunteers with braces and dental splints, careful instruction of the healthy volunteers, and by correcting the DWIs using Topup. However, dental work involving metals remains an issue, especially regarding the clinical use of this scan protocol. Fortunately, orthodontic braces and wires are generally not present in the intended patient population for this scan protocol, which is generally older than 50 years. Most dental materials used in these patients, such as amalgam and zirconia, do not induce severe inhomogeneity artifacts.

The main limitation of our study is the lack of a gold standard to which ex vivo and in vivo muscle CSD can validated, although the presented tractography appears to agree with results previously reported in the literature. Anatomical dissection including microscopy[6,27] has been able to resolve crossing muscle fibers; however, this technique is time-consuming, cannot be performed in vivo, and issues arise with the reconstruction into a 3D volume. Another limitation to the study is the participation of relatively young healthy volunteers without any dental prosthetics, which cause inhomogeneity artifacts and are often present in tongue cancer patients. Because these patients are generally in their sixth decade of life, and because the tongue composition changes with age due to muscular atrophy and lipomatosis,[40] care has to be taken to extrapolate the present results to the patient population. Finally, the scan protocol has not been validated for tongue cancer patients, where the diffusion signal may be affected by tumor infiltration and inflammation.

In conclusion, we have shown that the muscular architecture of the human tongue could be reconstructed in vivo in a clinically acceptable scan time. The present tractography results agreed with textbook anatomy. In the future, the proposed scan protocol may improve our understanding of how the complex muscular architecture of the tongue relates to tongue functionality after surgery for tongue cancer.

References

1. Sowder JC, Cannon RB, Buchmann LO, et al. Treatment-related determinants of survival in early-stage (T1-2N0M0) oral cavity cancer: A population-based study. Head Neck 2017;39:876–880.

2. Nicoletti G, Soutar DS, Jackson MS, Wrench AA, Robertson G, Robertson C. Objective assessment of speech after surgical treatment for oral cancer: Experience from 196 selected cases. Plast Reconstr Surg 2004;113:114–25.

3. Nicoletti G, Soutar DS, Jackson MS, Wrench AA, Robertson G. Chewing and swallowing after surgical treatment for oral cancer: Functional evaluation in 196 selected cases. Plast Reconstr Surg 2004;114:329–338.

4. Pauloski BR, Logemann JA, Colangelo LA, et al. Surgical variables affecting speech in treated patients with oral and oropharyngeal cancer. Laryngoscope 1998;108:908–916.

5. Kier WM, Smith KK. Tongues, tentacles and trunks: The biomechanics of movement in muscular-hydrostats. Zool J Linn Soc 1985;83:307–324.

6. Takemoto H. Morphological analyses of the human tongue musculature for three-dimensional modeling. J Speech Lang Hear Res 2001;44: 95–107.

7. Sanders I, Mu L. A three-dimensional atlas of human tongue muscles. Anat Rec 2013;296:1102–1114.

8. Kreeft A, Tan IB, van den Brekel MWM, Hilgers FJ, Balm AJM. The surgical dilemma of "functional inoperability" in oral and oropharyngeal cancer: Current consensus on operability with regard to functional results. Clin Otolaryngol 2009;34:140–146.

9. Gaige TA, Benner T, Wang R, Wedeen VJ, Gilbert RJ. Three dimensional myoarchitecture of the human tongue determined in vivo by diffusion tensor imaging with tractography. J Magn Reson Imaging 2007;26: 654–661.

10. Cleveland G., Chang DC, Hazelwood CF, Rorschach HE. Nuclear magnetic resonance measurement of skeletal muscle. Biophys J 1976;16: 1043–1053.

11. Van Donkelaar CC, Kretzers LJ, Bovendeerd PH, et al. Diffusion tensor imaging in biomechanical studies of skeletal muscle function. J Anat 1999;194:79–88.

12. Froeling M, Nederveen AJ, Heijtel DFR, et al. Diffusion-tensor MRI reveals the complex muscle architecture of the human forearm. J Magn Reson Imaging 2012;36:237–48.

13. Tournier J-D, Calamante F, Connelly A. Robust determination of the fibre orientation distribution in diffusion MRI: Non-negativity constrained super-resolved spherical deconvolution. Neuroimage 2007;35: 1459–1472.

14. Tournier JD, Calamante F, Gadian DG, Connelly A. Direct estimation of the fiber orientation density function from diffusion-weighted MRI data using spherical deconvolution. Neuroimage 2004;23:1176–1185.

15. Tuch DS, Reese TG, Wiegell MR, Makris N, Belliveau JW, Van Wedeen J. High angular resolution diffusion imaging reveals intravoxel white matter fiber heterogeneity. Magn Reson Med 2002;48:577–582.

16. Andersson JLR, Skare S, Ashburner J. How to correct susceptibility distortions in spin-echo echo-planar images: Application to diffusion tensor imaging. Neuroimage 2003;20:870–88.

17. Jones DK, Horsfield MA, Simmons A. Optimal strategies for measuring diffusion in anisotropic systems by magnetic resonance imaging. Magn Reson Med 1999;42:515–25.

18. Andersson JLR, Sotiropoulos SN. An integrated approach to correction for off-resonance effects and subject movement in diffusion MR imaging. Neuroimage 2016;125:1063–1078.

19. Yushkevich PA, Piven J, Hazlett HC, et al. User-guided 3D active contour segmentation of anatomical structures: Significantly improved efficiency and reliability. Neuroimage 2006;31:1116–1128.

20. Chang L-C, Jones DK, Pierpaoli C. RESTORE: Robust estimation of tensors by outlier rejection. Magn Reson Med 2005;53:1088–1095.

21. Leemans A, Jeurissen B. ExploreDTI: A graphical toolbox for processing, analyzing, and visualizing diffusion MR data. Proc Int Soc Magn Reson Med 2009;245:3300.

22. Froeling M, Nederveen AJ, Nicolay K, Strijkers GJ. DTI of human skeletal muscle: The effects of diffusion encoding parameters, signal-to-noise ratio and T2 on tensor indices and fiber tracts. NMR Biomed 2013;26:1339–1352.

23. Smith RE, Tournier JD, Calamante F, Connelly A. SIFT: Spherical-deconvolution informed filtering of tractograms. Neuroimage 2013;7:298–312.

24. Christensen RHB. Ordinal — Regression models for ordinal data. R package version 2018:8–25.

25. Gray H. Muscles of the tongue. In: Lewis WH (ed.). *Anatomy of the human body*, 20th ed. Philadelphia: Lea & Febiger; 1918:1128–1131.

26. Gilbert RJ, Wedeen VJ, Magnusson LH, et al. Three-dimensional myoarchitecture of the bovine tongue demonstrated by diffusion spectrum magnetic resonance imaging with tractography. Anat Rec A Discov Mol Cell Evol Biol 2006;288:1173–82.

27. Gaige TA, Kwon HS, Dai G, et al. Multiscale structural analysis of mouse lingual myoarchitecture employing diffusion spectrum magnetic resonance imaging and multiphoton microscopy. J Biomed Opt 2008;13:064005–064005.

28. Taylor EN, Hoffman MP, Aninwene GE 2nd, Gilbert RJ. Patterns of intersecting fiber arrays revealed in whole muscle with generalized Q-space imaging. Biophys J 2015;108:2740–2749.

29. Wedeen VJ, Hagmann P, Tseng W-YI, Reese TG, Weisskoff RM. Mapping complex tissue architecture with diffusion spectrum magnetic resonance imaging. Magn Reson Med 2005;54:1377–1386.

30. Tournier JD, Yeh CH, Calamante F, Cho KH, Connelly A, Lin CP. Resolving crossing fibres using constrained spherical deconvolution: Validation using diffusion-weighted imaging phantom data. Neuroimage 2008;42:617–625.

31. Murano EZ, Shinagawa H, Zhuo J, et al. Application of diffusion tensor imaging after glossectomy. Otolaryngol Head Neck Surg 2010;143:304–306.

32. Shinagawa H, Murano EZ, Zhuo J, et al. Tongue muscle fiber tracking during rest and tongue protrusion with oral appliances: A preliminary study with diffusion tensor imaging. Acoust Sci Technol 2008;29:291–294.

33. Ye C, Murano E, Stone M, Prince JL. A Bayesian approach to distinguishing interdigitated tongue muscles from limited diffusion magnetic resonance imaging. Comput Med Imaging Graph 2015;45:63–74.

34. Froeling M, Oudeman J, van den Berg S, et al. Reproducibility of diffusion tensor imaging in human forearm muscles at 3.0 T in a clinical setting. Magn Reson Med 2010;64:1182–90.

35. Tax CMW, Jeurissen B, Vos SB, Viergever MA, Leemans A. Recursive calibration of the fiber response function for spherical deconvolution of diffusion MRI data. Neuroimage 2014;86:67–80.

36. Tournier JD, Calamante F, Connelly A. Determination of the appropriate b value and number of gradient directions for high-angular-resolution diffusion-weighted imaging. NMR Biomed 2013;26:1775–1786.

37. Lingala SG, Zhu Y, Kim Y, Toutios A, Narayanan S, Nayak KS. A fast and flexible MRI system for the study of dynamic vocal tract shaping. Magn Reson Med 2016;1:112-125.

38. Alexander AL, Lee JE, Mariana Lazar ASF. Diffusion tensor imaging of the brain. Neurotherapeutics 2007;4:316.

39. Takemoto H. Morphological analyses and 3d modeling of the tongue musculature of the chimpanzee (*Pan troglodytes*). Am J Primatol 2008;70:966–975.

40. Bässler R. Histopathology of different types of atrophy of the human tongue. Pathol Res Pract 1987;182:87–97.